Epicyclic Gear Dynamics

Linda Smith Boyd* and James Pike†
United Technologies Corporation, Windsor Locks, Connecticut

A summary of a computer program and sample results are presented that predict the dynamic gear tooth load response for single-stage epicyclic gearing systems. The model used is an extension of the Richardson model developed in 1958 and the high-contact-ratio enhancements made by Cornell and Westervelt in 1978. The program has a preprocessor that will generate all the necessary geometric data for solving the system dynamics with a minimum of user input data. The program has the capability of modeling symmetric and buttressed, external and internal spur gear teeth, as well as the helical tooth form. Tooth profile modifications, planet gear phasing, gear tooth runout, and spacing errors can be modeled and evaluated. Summary tables are generated along with plotted data for dynamic tooth loads, flash temperatures, tooth bending stresses, hertz stresses, etc. The program also includes options for evaluating a floating input pinion, a flexible planet carrier, or a flexible ring gear, and the system natural frequencies. A speed survey option is also available to find peak dynamic loads.

Nomenclature

A,B,C,D = gear tooth coefficients
C = single-tooth pair compliance
C_0 = single-tooth pair compliance at pitch radius
d_{rp_i}, d_{sp_i} = tooth pair damping, lb·s/in.
d_x, d_y = damping at sun center in x and y directions
$e_{rp_{ij}}, e_{sp_{ij}}$ = tooth spacing error
J = polar moments of inertia
$[K]$ = stiffness matrix
K_{c_i}, K_{r_i} = segment stiffness
$\bar{K}_{c_i}, \bar{K}_{r_i}$ = pin stiffness
k_{rp_i}, k_{sp_i} = tooth pair stiffness, $k_{rp_i} = \eta_{rp_{ij}}\phi_{rp_{ij}}$ and $k_{sp_i} = \eta_{sp_{ij}}\phi_{sp_{ij}}$
k_x, k_y = spring rate at sun center in x and y directions
L_{rp_i}, L_{sp_i} = tooth pair loads for planet mesh i
L/W = load per unit face width
$[M]$ = mass matrix
m = translational mass of the sun gear
m_{c_i} = rotational (equivalent) mass of the planet carrier, $J_{c_i}/(R_{b_{c_i}})^2 + m_{p_i}/\cos^2\Phi$
$\mathrm{m}_{p_i}, \mathrm{m}_{r_i}$ = rotational (equivalent) mass of planet i and ring gear segment, $m_{p_i} = J_{p_i}/(R_{b_{p_i}})^2$ and $m_{r_i} = J_{r_i}/(R_{b_{r_i}})^2$
m_s = rotational (equivalent) mass of the sun gear, $J_s/(R_{b_s})^2$
N = number of planets
n = current tooth number
P = Benedict-Kelley parameter
Q = function of several parameters[1]
S = motion along line of action from pitch line
S_0 = reference distance along line of contact
T_f = flash temperature, °F
T_I = inlet oil temperature, °F
u_O = absolute viscosity of oil, MIL-L-23699 or -7808
V = sliding velocity
V_t = sum velocity
x,y = displacement of the sun center in x and y directions
X_{LOA} = sun-planet displacement along the line of action due to the floating sun
y_{c_i}, y_{p_i} = displacement along the line of action, $y_{c_i} = R_{b_{c_i}}\theta_{c_i}$ and $y_{p_i} = R_{b_{p_i}}\theta_{p_i}$
y_{r_i}, y_s = displacement along the line of action, $y_{r_i} = R_{b_{r_i}}\theta_{r_i}$ and $y_s = R_{b_s}\theta_s$
y_{rp_i}, y_{sp_i} = tooth pair displacement along the line of action, $y_{rp_i} = y_{p_i} - y_{r_i} - y_{c_i}$ and $y_{sp_i} = y_{s_i} - y_{p_i} - y_{c_i}$
Z_k = kinematic viscosity of oil
α_i = $\theta_c + \psi_i - \Phi$ (planetary)
α_i = $\psi_i - \Phi - \theta_r$ (star)
$\beta_{rp_{ji}}$ = cam modification, ring-planet mesh
$\beta_{sp_{ji}}$ = cam modification, sun-planet mesh
Δ_{rs} = spacing error for runout
Δ_r = input sun center displacement error
η_{rp_i} = ring-planet tooth pair spring rates
η_{sp_i} = sun-planet tooth pair spring rates
θ_{c_i} = carrier angle of rotation
θ_{r_i} = ring angle of rotation
λ = ω^2
μ = coefficient of friction
ρ = specific gravity of oil
τ_{in} = input torque
τ_{out} = output torque
Φ = pressure angle
$\phi_{rp_{ji}}$ = identity function for ring-planet tooth pair contact
$\phi_{sp_{ji}}$ = identity function for sun-planet tooth pair contact
χ_{sp} = 0 or 1 depending on whether the tooth contact is on the profile modification cam or not
ψ_i = relative angular position of planets, = $2\pi(i-1)/N$, $i = 1,2,3,\ldots,N$
ω = natural frequency, rad/s

Subscripts

c = carrier
i = planet mesh
j = tooth pair mesh, ≤ 4
p = planet gear
r = ring gear

Received June 19, 1987; presented as Paper 87-2042 at the AIAA/SAE/ASME/ASEE 23rd Joint Propulsion Conference, San Diego, CA, June 29–July 2, 1987; revision received May 5, 1988.

*Analytical Engineer, Hamilton Standard Division. Member AIAA.

†Head of Applied Mechanics, Hamilton Standard Division. Member AIAA.

rp = ring-planet tooth pair mesh
s = sun gear
sp = sun-planet tooth pair mesh

Introduction

EFFICIENT and minimum weight transmission systems have been gear designers' goals for many years, especially in the aircraft/aerospace industry. Generally, a major design consideration is gearing dynamics, specifically gear tooth meshing dynamics. In high-powered transmissions the gear tooth meshing dynamics will influence gear box generated noise, gear tooth fatigue life, and general gear box dynamics. Therefore, gearing tooth dynamic prediction techniques are desirable during the transmission design phase.

A gear tooth dynamics prediction code[1-4] has been developed during the last several years. This development has evolved to a single-stage epicyclic gear dynamics prediction code that can model a wide range of design parameters. A discussion of that development work is given here.

Program History

The epicyclic gear dynamics program determines detailed gear tooth geometry, dynamic tooth loads, stresses, and surface damage factors for single-mesh and epicyclic gear systems with internal, external, buttress, or helical involute tooth forms. The significant parameters can be plotted through the entire mesh with the maximum values output in tabular form.

The initial program was for a single spur gear mesh and was developed to operate over a wide range of contact ratios (up to 4.0) to analyze high-contact as well as low-contact ratio gearing. This single-mesh program was an extension, by Cornell and Westervelt,[5,6] of the basic concept developed by Richardson in 1958.[7]

The tooth pair compliance and stress sensitivity formulation of the single spur gear mesh program is used in the epicyclic gear dynamics program, applied to each tooth pair mesh. The basic external involute tooth form was also extended to include buttress and internal involute tooth forms. The teeth may be modeled with modified involute profiles and spacing errors as well as runout errors.

The program also includes variable contact friction as a function of sliding velocity throughout each mesh, user-friendly features, dynamic side bands generated from gear runout, and a speed survey option for locating peak responses. The most recent modifications include additional degrees of freedom to include a flexible ring gear rim, a flexible planet carrier, and a floating sun gear. In addition, a natural frequency option to solve for undamped eigenvalues and eigenvectors was added, as well as the framework for a finite-element compliance formulation for helical gear teeth.

The program is summarized by the flowchart of Fig. 1.

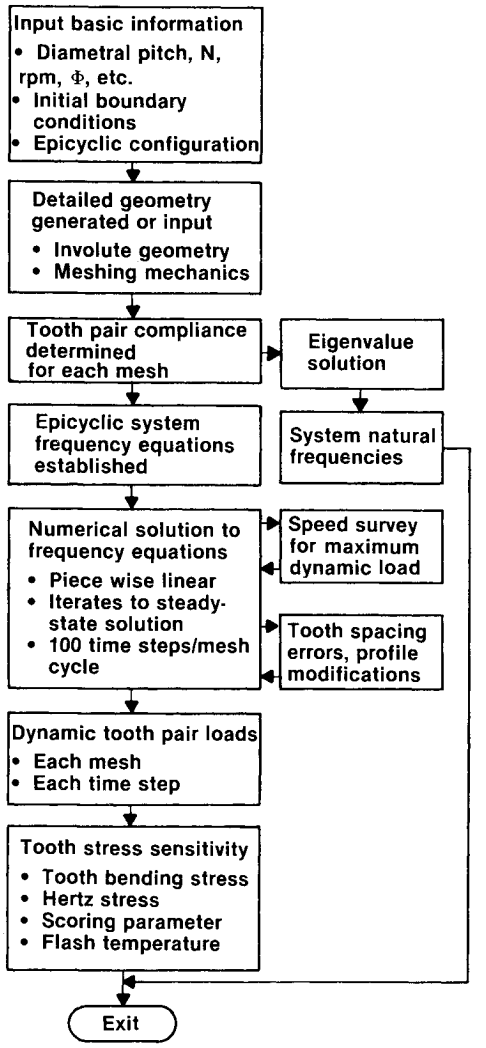

Fig. 1 Flowchart of epicyclic gear dynamic program.

Dynamic Model

The analysis uses a system of dynamic equations to solve for the tooth pair displacements along the respective mesh lines of action as a function of time. This assumes any radial component of motion is secondary to the tooth pair motion along the line of action. The dynamic model for an epicyclic system is shown in Fig. 2. The equations of motion for each component of the N planet system are as follows.

Sun gear:

$$m_s\ddot{y}_s + \sum_{i=1}^{N} d_{sp_i}\dot{y}_{sp_i} + \sum_{i=1}^{N} L_{sp_i} = \frac{\tau_{\text{in}_s}}{R_{b_s}} \tag{1}$$

Planet gear i:

$$m_{p_i}\ddot{y}_{p_i} - d_{sp_i}\dot{y}_{sp_i} + d_{rp_i}\dot{y}_{rp_i} - L_{sp_i} + L_{rp_i} = 0 \tag{2}$$

Ring gear segment i:

$$m_{r_i}\ddot{y}_{r_i} - d_{rp_i}\dot{y}_{rp_i} - L_{rp_i} + K_{r_i}(y_{r_i} - y_{r_{i+1}}) + K_{r_{i-1}}(y_{r_i} - y_{r_{i-1}}) = -\bar{K}_{r_i}y_{r_i} \tag{3}$$

Carrier segment i:

$$m_{c_i}\ddot{y}_{c_i} - d_{rp_i}\dot{y}_{rp_i} - d_{sp_i}\dot{y}_{sp_i} - L_{rp_i} - L_{sp_i} + K_{c_i}(y_{c_i} - y_{c_{i+1}}) + K_{c_{i-1}}(y_{c_i} - y_{c_{i-1}}) = -\bar{K}_{c_i}y_{c_i} \tag{4}$$

where

$$\sum_{i=1}^{N} \bar{K}_c y_{c_i} = \frac{\tau_{\text{out}}}{R_{b_c}} \tag{5a}$$

$$\sum_{i=1}^{N} \bar{K}_r y_{r_i} = \frac{\tau_{\text{out}}}{R_{b_r}} \tag{5b}$$

These equations are for a differential epicyclic system [$3N + 1$ degrees of freedom (DOF)] where the ring and planet carrier are free to rotate. The number of equations and DOF are reduced for other epicyclic systems solved in the program. For a planetary system, the ring gear is fixed and thus Eq. (3) is eliminated ($2N + 1$ DOF). Similarly, Eq. (4) is eliminated for a star system where the planet carrier is fixed. If a rigid gear rim ($K_r = \infty$) or rigid carrier ($K_c = \infty$) for a star or planetary,

Table 1 Floating sun test case results

Planet no.	k_x, lb/in. (N/cm)	k_y, lb/in. (N/cm)	d_x, lb·s/in. (N · s/cm)	d_y, lb·s/in. (N · s/cm)	Maximum load Sun-planet lb	Sun-planet N	Ring-planet lb	Ring-planet N	Percent difference from nonflexible maximum load, % Sun-planet	Ring-planet
1	–	–	–	–	19.13	85.09	17.05	75.84		
2	–	–	–	–	19.19	85.36	15.85	70.50		
3	–	–	–	–	19.32	85.94	16.03	71.30		
1	10.0×10^6	10.0×10^6	0.05	0.05	20.42	90.83	19.44	87.46	6.7	14.0
2	(17.5×10^6)	(17.5×10^6)	(0.088)	(0.088)	20.34	90.47	18.08	80.42	6.0	14.1
3					19.68	87.54	18.47	82.15	1.9	15.2
1	30.0×10^6	30.0×10^6	0.02	0.02	19.26	85.67	17.77	79.04	0.68	4.2
2	(52.6×10^6)	(52.6×10^6)	(0.035)	(0.035)	19.72	87.71	16.57	73.70	2.8	4.5
3					19.64	87.36	16.95	75.40	1.7	5.7

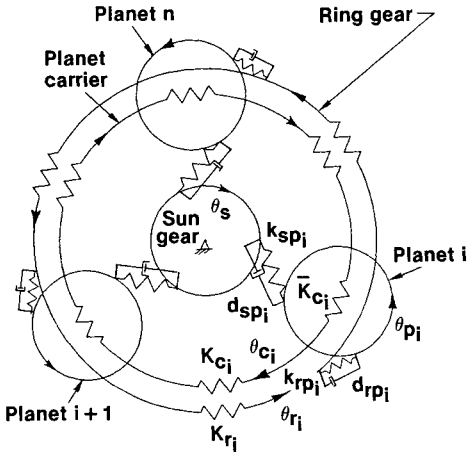

Fig. 2 Dynamic model for epicyclic gear system.

respectively, is assumed, Eqs. (3) or (4) can be reduced from N equations to one equation ($N + 2$ DOF).

A numerical solution is time stepped through the mesh, solving for the dynamic loads from the equations of motion. To obtain a steady-state solution, the dynamic solution is iterated until the displacement and velocity boundary conditions converge for the tooth pair meshes. Convergence is determined by comparing the tooth pair displacements and velocities along the lines of action at the beginning and end of a mesh cycle until the values differ by less than a specified tolerance for a case with no tooth errors.

Tooth Pair Compliance

The tooth pair stiffness terms vary as the load location changes in the mesh cycle. The general compliance formulas for the gear teeth are developed in Refs. 5 and 6 and consist of three contributions: 1) the basic tooth as a cantilever beam, 2) the fillet and foundation effects, and 3) the local contact compression. These are determined for seven load positions for each tooth pair and combined to obtain the following fourth-order polynomial for compliance as a function of position along the line of action:

$$C = C_0[1 + A(S/S_0) + B(S/S_0)^2 + C(S/S_0)^3 + D(S/S_0)^4] \quad (6)$$

This gives the general tooth pair compliance for any load location and corresponding time in the mesh cycle.

Floating Sun Gear Option

The floating sun gear option adds two additional DOF at the sun center. The equations of motion for the sun gear center in Cartesian coordinates, x and y directions, using the model of Fig. 3, can be written as

$$m\ddot{x} + d_x\dot{x} + k_x x - \sum_{i=1}^{N} d_{sp_i}\dot{y}_{sp_i}\sin\alpha_i - \sum_{i=1}^{N} L_{sp_i}\sin\alpha_i = 0 \quad (7)$$

$$m\ddot{y} + d_y\dot{y} + k_y y + \sum_{i=1}^{N} d_{sp_i}\dot{y}_{sp_i}\cos\alpha_i + \sum_{i=1}^{N} L_{sp_i}\cos\alpha_i = 0 \quad (8)$$

where

Planetary system:

$$\alpha_i = \theta_c + \psi_i - \Phi \quad (9a)$$

Star system:

$$\alpha_i = \psi_i - \Phi - \theta_r \quad (9b)$$

The angle α_i is for resolution of the tooth pair forces from along the line of action to the Cartesian coordinates x and y.

The tooth pair meshing loads are determined from

$$L_{sp_i} = \sum_{j=1}^{m}[(y_{sp_i} - e_{sp_{ji}} - \chi^2_{sp_{ji}}\beta^2_{sp_{ji}} + X_{\mathrm{LOA}_i})\eta_{sp_{ji}}\phi_{sp_{ji}}] \quad (10)$$

$$L_{rp_i} = \sum_{j=1}^{m}[(y_{rp_i} - e_{rp_{ji}} - \chi^2_{rp_{ji}}\beta^2_{rp_{ji}})\eta_{rp_{ji}}\phi_{rp_{ji}}] \quad (11)$$

where

$$X_{\mathrm{LOA}_i} = y\cos\alpha_i - x\sin\alpha_i \quad (12a)$$

and for rigid sun mounts

$$x_{\mathrm{LOA}_i} = 0 \quad (12b)$$

Table 1 illustrates the effects of a floating sun on the dynamic tooth loads compared to a hard-mounted system with characteristics shown in Table 2. For this particular case, up to 15% load difference occurs.

Natural Frequency Option

The natural frequency option allows the user to investigate natural frequencies of the system through a classical eigenvalue solution. The effects of various spring rates at the sun center for a floating sun, or the effect of various stiffnesses of a planet carrier and/or ring gear rim on the frequency response, can be readily determined. In addition, by using the planet phasing constants, the range of frequencies due to the nonlinear tooth meshing action can be investigated.

The general form of the dynamic equations for the eigenvalue solution is

$$[M]\{\ddot{x}\} + [K]\{x\} = 0 \quad (13)$$

Table 2 Nonsynchronous planetary system characteristics

No. of planets	3			
Diametral pitch	1/3			
Module	3			
Pressure angle	22.5 deg			
Static load	29.25 lb (130 N)			
Tooth pair error 0.0001334 in. (0.003388 mm)				
	Sun	Planets	Ring	Carrier
No. of teeth	14	28	70	–
Face width, in.	1.18	1.18	1.42	–
mm	30.0	30.0	36.0	–
Equivalent mass				
lb	0.056	0.155	0.0	28.9
kg	0.0255	0.0704	0.0	13.12

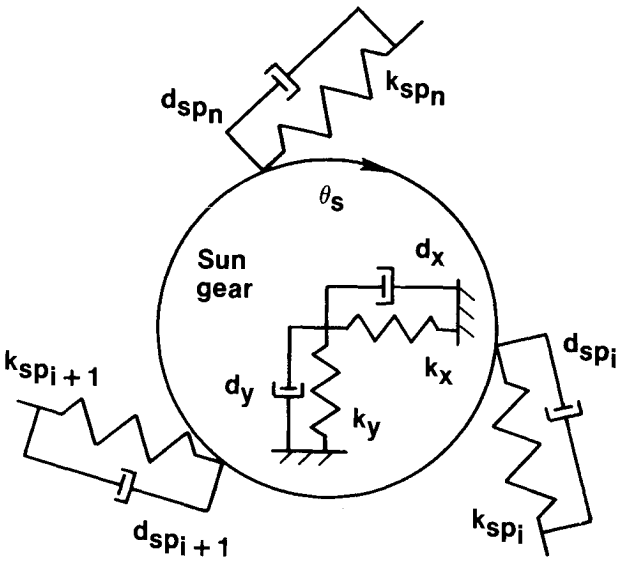

Fig. 3 Dynamic model for floating sun gear.

The mass and stiffness matrices $[M]$ and $[K]$ are derived from the system of Eqs. (1) to (4) and, optionally, Eqs. (7) and (8). The eigenvector/eigenvalue solution then solves for the roots of the determinant:

$$[K] - \lambda[M] = 0 \tag{14}$$

A standard eigenvalue/eigenvector numerical solution routine for real, symmetric matrices is used to solve the determinant.

The natural frequency option can be used for eight system types: planetary, star, differential, single meshes, planetary with flexible carrier, star with flexible ring gear rim, or differential system with both a flexible ring gear rim and a flexible planet carrier. In addition, the floating sun DOF can be included in the solution.

The frequency solution uses tooth pair stiffnesses from the nonlinear compliance formulation of the gear program. The solution is for a specific instant in time, with the corresponding tooth pair stiffnesses. This compliance formulation also includes the Hertzian effect; thus, the torque that is input will influence the natural frequencies. A zero torque case will eliminate the Hertzian effect if it is not desired.

Variable Contact Friction

Modifications have been made to the program to internally calculate the coefficient of friction as a variable throughout the mesh. The coefficient of friction is a function of the Benedict-Kelley parameter,[8]

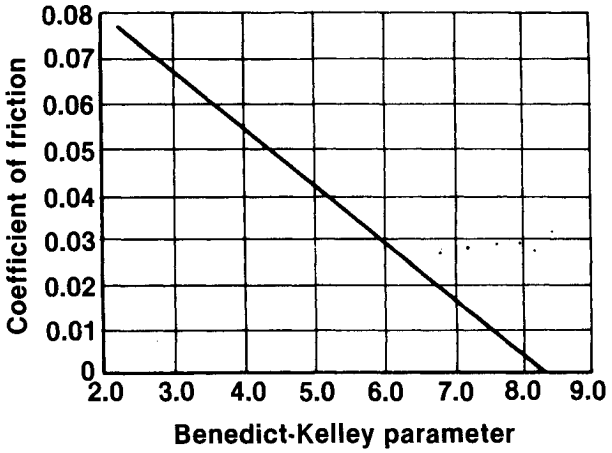

Fig. 4 Benedict-Kelley coefficient of friction.

$$P = \log_{10}[u_0 V V_t^2/(L/W)] \tag{15}$$

This is a function of the load per unit face width, sum velocity, sliding velocity, and absolute viscosity of the oil.

The empirical equation for coefficient of friction representing the data points presented by Benedict and Kelley[8] is shown in Fig. 4 and is

$$\mu = -0.0130556(P) + 0.10933 \tag{16}$$

The absolute viscosity u_0 used for the above expression must be input to the program via an oil type. The other variables are already available in the program. The absolute viscosity as a function of oil inlet temperature is given by

$$u_0 = \rho Z_k \tag{17}$$

The coefficient of friction influences the flash temperature T_f by the equation

$$T_f = T_i + Q_\mu \tag{18}$$

A comparison case was executed using a single sun-planet mesh. The calculated coefficients of friction are less than the 0.05 that would have been assumed without the Benedict-Kelley formulation. Thus, the new flash temperatures are lower and should be more realistic. Figure 5a shows the flash temperatures for the constant friction coefficient, while Fig. 5b shows the variable coefficient of friction flash temperatures.

The epicyclic program also calculates an average coefficient of friction throughout the mesh for each sun-planet and ring-planet mesh.

Dynamic Side Bands

Dynamic side bands are observed in frequency spectra where they usually occur in plus or minus integer multiples of the primary gear mesh frequency. This phenomenon is often associated with inherent manufacturing errors, such as gear runout.

For the sideband option, runout errors are simulated by applying a sinusoidal error distribution on the input pinion. The user inputs the displacement deviation in the center location of the sun. Then this is used to generate a tooth spacing error array using the following equation:

$$\Delta_{r_s} = \Delta_r \sin[2\pi(n/N_s)] \sin\Phi \tag{19}$$

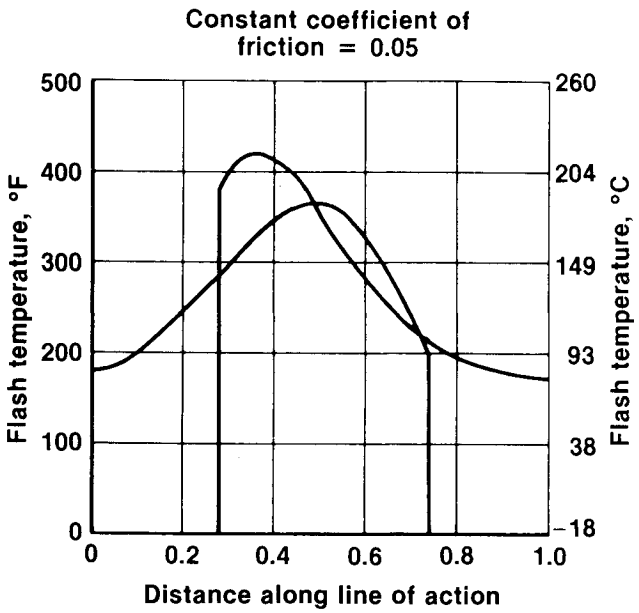

Fig. 5a Flash temperatures with constant coefficient of friction.

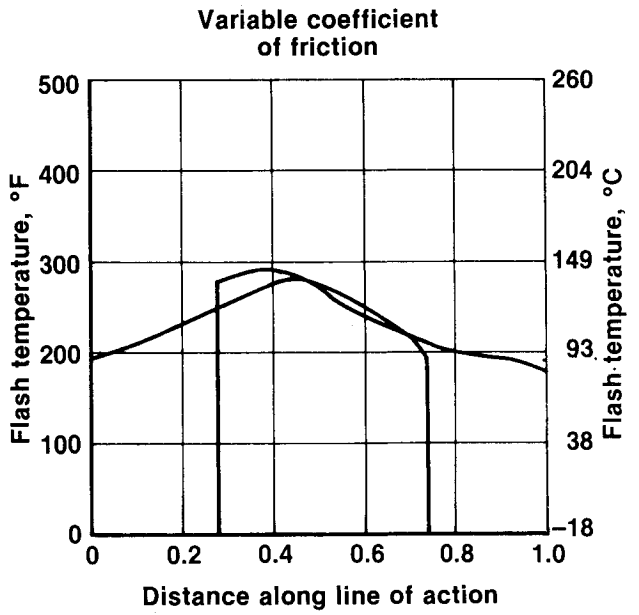

Fig. 5b Flash temperatures with variable coefficient of friction.

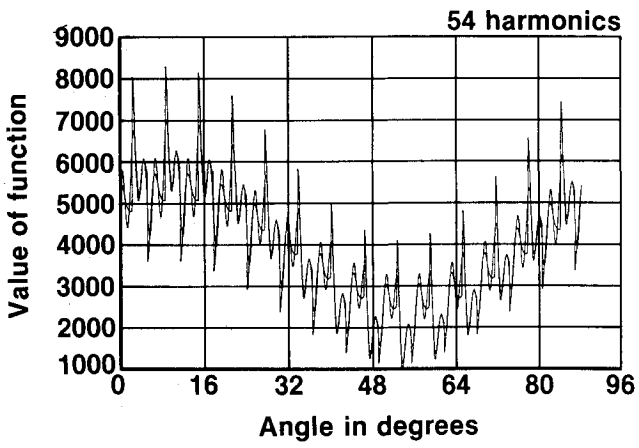

Fig. 6 Runout loads vs angular location on pinion.

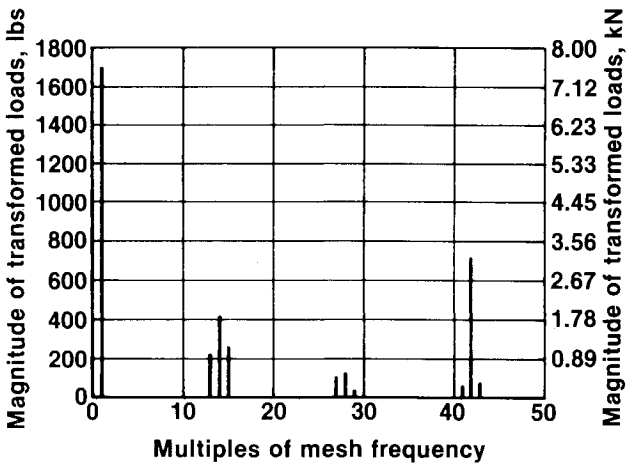

Fig. 7 Fourier transformed loads vs order of harmonics.

An error array is internally generated and the tooth loads calculated for each tooth of the sun-planet mesh.

In order to obtain sideband information, the load data must be used in conjunction with a Fourier analysis in order to observe the results in the frequency domain. The program writes all of the loads and corresponding times to an output file so the data can be analyzed separately.

An example case was executed with an error of 0.001 in. The maximum normal load varied from 3045–5723 lb, whereas the no-error maximum load was 4387 lb. The load data shown in Fig. 6 was used in conjunction with a Fourier analysis program to obtain the loads shown in Fig. 7.

Helical Tooth Form

The program offers two options for analyzing helical tooth forms. The first method uses a segmental spur gear configuration where the tooth is divided into 10 segments, each of which is evaluated as if it were an independent spur tooth. This is a first-order approximation because it neglects the coupling of the neighboring segments.

The second option incorporates a finite-element model for obtaining a compliance curve of the same form as Eq. (6). The basic ground work for a complete finite-element solution has been incorporated, but it has not been fully developed or evaluated. The routines need to be used more fully, especially with respect to stress postprocessing and finite-element stiffness interaction with the dynamic solution. The stress postprocessing currently uses the spur gear routine that inherently assumes the load line is parallel to the axis of rotation.

Evaluation

The analytical method was evaluated by comparing some of the program results with published test data. There is little published test data of sufficient detail, with the exception of a series of articles published in the Bulletin of the Japanese Society of Mechanical Engineers.[9-11] The articles document experimental investigations into dynamic tooth loading in Stoeckicht 2K-H planetary gears. Comparison of the test data for the planetary system with the theory showed the loads correlated well.

Two systems were tested, one with synchronous meshing and one with nonsynchronous meshing. The systems were designed for 20 kW of transmitted power, speed ratio of 6, and working range of the higher-speed shaft of 1800–7200 rpm. The two systems were kept as similar as possible, with the major changes being diametral pitch and number of teeth, in order to make a direct comparison between systems with the major difference being the planet phasing.[9] The basic characteristics of the systems are in Tables 2 and 3.

Table 3 Synchronous planetary system characteristics

No. of planets	3			
Diametral pitch	0.5			
Module	2			
Pressure angle	22.5 deg			
Static load	29.25 lb (130 N)			
Tooth pair error 0.0001334 in. (0.003388 mm)				
	Sun	Planets	Ring	Carrier
No. of teeth	21	42	105	–
Face width, in.	1.18	1.18	1.18	–
mm	30.0	30.0	30.0	–
Equivalent mass				
lb	0.056	0.155	0.0	28.9
kg	0.0255	0.0704	0.0	13.12

Figure 8 illustrates the maximum dynamic loads for a static tangential tooth load of 130 N (28.25 lb) for the nonsynchronous meshing case. The dynamic load is defined as the ratio of the dynamic strain to the static strain at corresponding positions, and the coefficient of variation of the dynamic load is the standard deviation divided by the mean dynamic load. The test data plotted are the mean load ± 2 times the standard deviation for a single tooth contact. The theoretical model of Ref. 8 is very similar to that used here. The primary differences are that the reference model included additional error terms and mass terms for rotor inertias but did not include the nonlinear tooth pair meshing characteristics. The effective masses are the same as the authors[10] used in their evaluation, with the carrier mass including the low-speed rotor effective mass. The results of their analysis are also shown in Fig. 8.

Figure 8 shows the nonsynchronous meshing system. The range of experimental strain gage results indicate a resonance near 2600 rpm, which is due to a resonance of the total torsional system resulting in torque variations.[9] The analytical program did not predict this resonance. The next resonance indicated experimentally is in the 5000 rpm vicinity. The program predicts a resonant speed at 5200 rpm.

Figure 9 illustrates the synchronous meshing system results. The theory predicts a resonance at approximately 7200 rpm, which is a multiple of the meshing frequency.[9] The experimental range does not indicate this significantly. Synchronous meshing can cause higher loads due to simultaneous meshing of the planets. This is shown by comparing Figs. 8 and 9, where both the experimental and analytical loads are high for the synchronous meshing case at the resonant speeds.

Figure 9, for the synchronous meshing case, shows the results for the same magnitude of error applied to one tooth in all three sun-planet meshes. At higher speeds, the effect of tooth spacing errors on dynamic loads is reduced. The loads plotted for the error case are the minimum and maximum. The maximum normally occurs in only one mesh, and the average increase in loads for the error cases would be considerably lower. The manufacturing errors were estimated in Ref. 7. The pitch error, profile error, and lead error were incorporated in a statistical total[4] for a sun-planet mesh of magnitude 0.003388 mm (0.00013338 in.) using

$$e = \sqrt{\sum_{\mu} e_{\mu}^2} \tag{20}$$

where e_{μ} is the various types of tooth errors.

Variation of the analytical effective mass has the effect of shifting the speed at which peak loads occur. The selection of effective masses for the analytical model is not a trivial task in that it is difficult to decide on the amount of attached mass that should be included. These attached masses could be rotors, shafting, mounts, etc. A complete system dynamic analysis would be required to define the equivalent masses, which are frequency dependent. The planetary gear tested contained

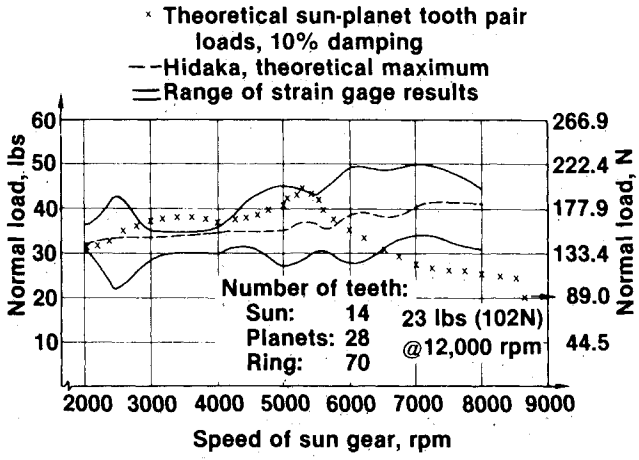

Fig. 8 Nonsynchronous planetary system.

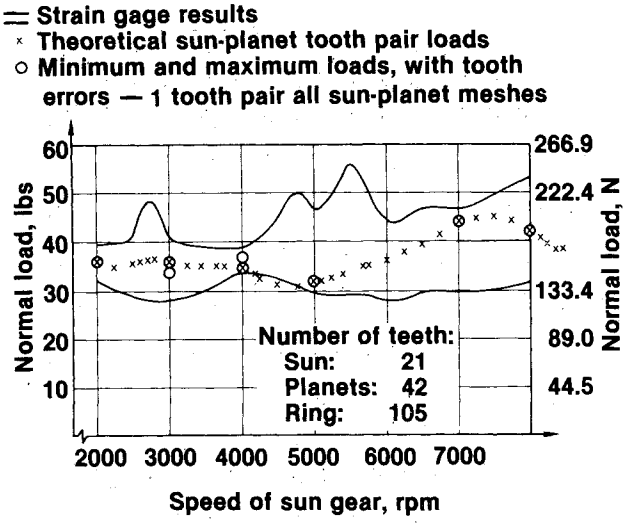

Fig. 9 Synchronous planetary system.

a high- and a low-speed rotor that were modeled by adding the additional mass to the ring gear and planet carrier, respectively. However, the ring is fixed for a planetary system and, therefore, has zero rotational moment of inertia and, correspondingly, zero effective mass. The actual system tested has a radially floating ring as well as a floating sun, neither of which was included in the theoretical model at the time of evaluation.

The masses used for the majority of the theoretical calculations are the masses given in Ref. 6. However, Fig. 10 illustrates the effect of varying the effective mass as well as variation of the damping ratio. The shift in the speed at which the peak load occurs, due to altered effective mass, is illustrated in Fig. 10. This shows the theoretical peak shifting from about 5300 rpm to approximately 7400 rpm when all masses are divided in half. The half-mass results seem to correlate with the experimental data better; however, there is insufficient information to verify either quantity as the actual effective mass.

In addition to the case where all effective masses are halved, a case where only the planet carrier mass was decreased also is shown in Fig. 10. There is a slight increase in loads and a slight shift in the main peak toward a higher speed. The differences in loads are less than 3%. Thus, in this case, the carrier effective mass is not the primary mass of the system in that speed range, even though it is the largest effective mass of the system.

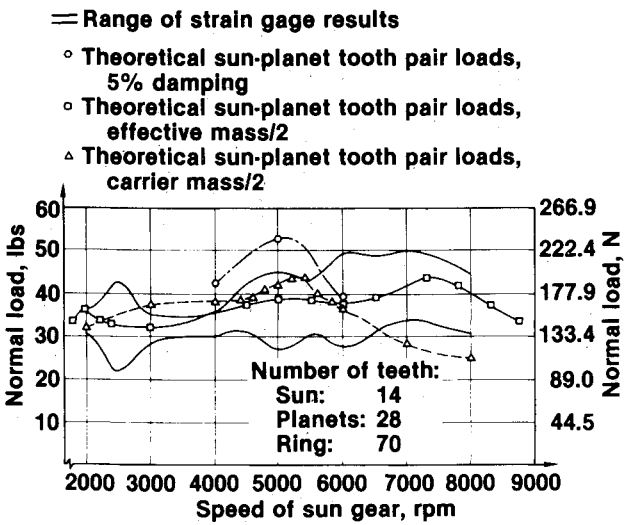

Fig. 10 Mass and damping variations for nonsynchronous planetary system.

Figure 10 also contains a few points at a much lower damping ratio of 5%. This increases the load at 5000 rpm by 26.5% and emphasizes the dynamic peak obtained near 5000 rpm. The Japanese theoretical calculations used a 10% damping ratio, which correlated well to the experimental test data.

Summary and Conclusions

The epicyclic gear program is a universal program that can analyze tooth pair loads for a wide variety of system types: planetary, star, single meshes, planetary with flexible carrier, or star with flexible ring gear rim. In addition, the floating sun DOF can be included in the solution. The following conclusions have been reached:

1) The comparison of the Stoeckicht 2K-H planetary system data with theory showed the loads correlated well.

2) The test system was shown to be very dependent on the equivalent masses and damping ratio input, with respect to resonant speeds and load magnitudes, respectively. This phenomenon is typical of lowly damped systems to vibratory loads. Therefore, a range of effective mass should be studied for sensitivity of dynamic response.

3) The program predicts the general location of the natural frequencies in the dynamic load solution as well as the eigenvalue solution. The effect of the meshing action of the teeth with nonlinear stiffness on the natural frequencies can be evaluated easily via the eigenvalue solution. The variable coefficient of friction modifications lead to more accurately predicted flash temperatures.

4) The dynamic side band option allows the user to investigate the simulated effect of a runout error on the input pinion of a single external-external tooth pair mesh. The number of error solutions calculated is equivalent to the number of teeth on the input pinion, simulating runout for a full mesh cycle. The load data can be used to obtain the frequency spectrum to evaluate the sideband phenomenon.

5) The program should be more thoroughly tested and evaluated via parametric studies as well as comparison to test data. Only a few test cases have been run for each option due to the minimum amount of epicyclic data available for comparison.

6) The epicyclic gear tooth dynamic analysis program provides the designer with a very useful tool with which he can optimize a gear tooth mesh, whether it be high- or low-contact-ratio gearing, standard or nonsymmetrical teeth, with or without tip relief.

Acknowledgment

The authors would like to thank Hamilton Standard, Division of United Technologies, for permission to publish this work and NASA Lewis Research Center, Cleveland, OH, for funding this program. They also would like to acknowledge the support from Dr. R. W. Cornell at Hamilton Standard and Dennis Towsend at NASA Lewis.

References

[1]Pike, J., "Interactive Multiple Spur Gear Mesh Dynamic Load Program," NASA CR-165514, Dec. 1981.

[2]Pike, J., "Expansion of the Dynamic Load Solution for Multiple Planet Spur Gearing to Helical Gearing," Doc. Rept. to NASA Lewis Research Center, Sept. 1983.

[3]Boyd, L. S. and Pike, J., "Multi-Mesh Gear Dynamics Program Evaluation and Enhancements," NASA CR-174747, Sept. 1984.

[4]Boyd, L. S. and Pike, J., "Expansion of Epicyclic Gear Dynamic Analysis Program," NASA CR-179563, Aug. 1986.

[5]Cornell, R. W., "Compliance and Stress Sensitivity of Spur Gear Teeth," *Journal of Mechanical Design,* Vol. 103, April 1981, pp. 447-459

[6]Cornell, R. W. and Westervelt, W. W., "Dynamic Tooth Loads and Stressing for High Contact Ratio Spur Gears," *Journal of Mechanical Design,* Jan. 1978, pp. 69-76.

[7]Richardson, H. H., "Static and Dynamic Load, Stresses, and Deflection Cycles in Spur-Gear Systems," Sc.D. Thesis, Massachusetts Institute of Technology, Cambridge, MA, 1958.

[8]Benedict, G. H. and Kelley, B. W., "Instantaneous Coefficients of Gear Tooth Friction," *ASLE Transactions,* Vol. 4, 1961, pp. 59-70.

[9]Hidaka, T., Terauchi, Y., and Nagamura, K., "Dynamic Behavior of Planetary Gear (6th Rept., Influence of Meshing-Phase)," *Bulletin of the JSME,* Vol. 22, No. 169, July 1979, pp,. 1026-1033.

[10]Hidaka, T., Terauchi, Y., and Fujii, M., "Analysis of Dynamic Tooth Load on Planetary Gear," *Bulletin of the JSME,* Vol. 23, No. 176, Feb. 1980, pp. 315-323.

[11]Hidaka, T., Terauchi, Y., and Dohi, K., "On the Relation Between the Run-Out Errors and the Motion of the Center of Sun Gear in a Stoeckicht Planetary Gear," *Bulletin of the JSME,* Vol. 22, No. 167, May 1979, pp. 748-754.